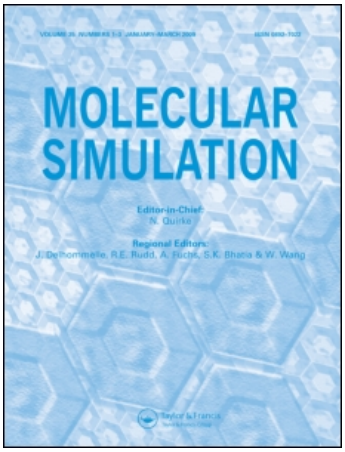

Molecular Simulation
Publication details, including instructions for authors and subscription information:
http://www.informaworld.com/smpp/title~content=t713644482

Simulation of quantum separation of binary hydrogen isotope mixtures in carbon slit pores

Yang Wang[a]; Suresh K. Bhatia[a]
[a] Division of Chemical Engineering, The University of Queensland, Brisbane, QLD, Australia

First published on: 21 September 2010

To cite this Article Wang, Yang and Bhatia, Suresh K.(2009) 'Simulation of quantum separation of binary hydrogen isotope mixtures in carbon slit pores', Molecular Simulation, 35: 1, 162 — 171, First published on: 21 September 2010 (iFirst)
To link to this Article: DOI: 10.1080/08927020802267394
URL: http://dx.doi.org/10.1080/08927020802267394

Molecular Simulation
Vol. 35, Nos. 1–2, January–February 2009, 162–171

Taylor & Francis
Taylor & Francis Group

Simulation of quantum separation of binary hydrogen isotope mixtures in carbon slit pores

Yang Wang and Suresh K. Bhatia*

Division of Chemical Engineering, The University of Queensland, Brisbane, QLD 4072, Australia

(*Received 26 May 2008; final version received 11 June 2008*)

The carbon slit pore has been investigated as a medium for low temperature hydrogen isotope mixture separation. It is shown that the path integral formalism with Silvera–Goldman potential provides the most accurate results for the adsorption simulations. At 40 K, an operating pressure of 1.0 bar and carbon slit width of 0.56 nm is found to be optimal for efficient quantum separation. Simulations for practical separation processes using a 99.95% H_2 and 0.05% D_2 bulk composition H_2/D_2 mixture, using the optimal carbon slit pore at 40 K and 1.0 bar, demonstrate that the deuterium mole fraction increases from 0.05 to 50.3% after three separation steps. The results show highly efficient equilibrium separation of binary H_2/D_2 mixtures in narrow carbon slit pores, indicating the potential of molecular sieving carbon materials for hydrogen isotope separations.

Keywords: hydrogen isotope separation; carbon slit pores; quantum effect

1. Introduction

The separation of hydrogen isotopes is a problem that is currently attracting much attention. In parti cular the heavier isotope, deuterium, is of much importance, with numerous applications such as nuclear fusion, non-radioactive isotopic tracing, neutron scattering and hydrogen nuclear magnetic resonance as well as a host of others. However, the natural abundance of deuterium is very low, at about 0.03%, and its separation is difficult as its thermodynamic properties are close to those of hydrogen. Currently popular separation methods, such as cryogenic distillation, centrifugal enrichment and electromagnetic mass spectrometry, are very expensive and high in energy cost. The development of a cost-effective separation method is therefore of great significance. In recent years, much work has been done to investigate quantum effects at low temperature, which can potentially be exploited to separate the isotopes [1–7]. Since deuterium is twice as heavy as hydrogen, the magnitude of the quantum effect encountered by it is lower than that for hydrogen at low temperature, opening up the possibility of exploiting this difference for separation.

Materials with nano-scale size pores can be a potential medium for quantum adsorption of light gases. Quantum separation becomes possible if the pore size is comparable to the size of the hydrogen molecule, as quantum effects can be enhanced in very confined environments, with differences in magnitude of the effect encountered by different isotopes. Many researchers have investigated quantum adsorption of hydrogen in nano-porous materials [1,3–5,7–14], with some focusing on the quantum separation of hydrogen isotopes. The possibility of exploiting quantum effects was first recognised by Beenakker et al. [15] who investigated a simple model of hard spheres in cylindrical pores, showing larger adsorption of deuterium due to quantum swelling of hydrogen. Subsequent simulations by Sholl and co-workers [1,2] using more realistic interactions have confirmed this effect. Kaneko and his co-workers [12–14] have verified the effect via both simulations and experiments. More recently, using both grand canonical Monte Carlo (GCMC) and molecular dynamics simulations, Bhatia and co-workers [3,4] have shown an even more remarkable effect that the heavier deuterium even diffuses faster than hydrogen at sufficient low temperatures in a zeolite molecular sieve as well as in $AlPO_4$-25 [5], raising the possibility of kinetic molecular sieving of these isotopes. This prediction has been subsequently and experimentally confirmed by Zhao et al. [16] using a 3 Å carbon molecular sieve. Thus, molecular sieving materials of suitable pore sizes would appear promising for this application.

Microporous carbons are relatively inexpensive nanoporous materials, and previous studies have shown their capability for hydrogen adsorption at low temperature [9,10,17]. However, such studies have predominantly investigated adsorption of only pure components, either H_2 or D_2. Challa et al. [1] have shown high selectivity of D_2 over H_2 from mixtures in nanotube systems. However, the narrow (3,6) and (6,6) nanotubes investigated in their calculations have yet to been isolated experimentally. The other sample material studied is interstices of (10,10) nanotube, however, such materials are still not available for commercial application. In addition, there are complexities in nanotube packing and system design, that make this route impractical at the present time. Therefore, studies for mixture adsorption and selectivity in more practical

*Corresponding author. Email: s.bhatia@eng.uq.edu.au

ISSN 0892-7022 print/ISSN 1029-0435 online

DOI: 10.1080/08927020802267394
http://www.informaworld.com

adsorbents are in need. A very recent study by Garberoglio [18] has shown high selectivity for the heavier isotopes in a narrow slit pore with size of 0.57 nm at a low temperature of 20 K. However, more detailed studies of the effect of slit pore size at various operating conditions of temperature and pressure are still lacking, and the optimal pore size yet to be determined.

Here we investigate the binary H_2/D_2 system in carbon slit pores, performing equilibrium simulations to study their quantum separation. There are two key techniques to account for the quantum effects in simulations. One method is the Feynman–Hibbs (FH) effective potential approximation [19–22], which considers the quantum particle as having a Gaussian spread. Previous studies have shown this method can reproduce the bulk phase properties of hydrogen very well [3,4] if interaction parameters are fitted. The other method is the Feynman's path integral (PI) formalism [23,24], in which each molecule is replaced by a ring of multiple-beads (ring polymer), which behaves classically. This method is considered to be accurate if a sufficiently large number of beads is taken for each molecule. Using this approach, thermodynamic properties and phase equilibrium of bulk phase hydrogen have been simulated and the results have been verified to be accurate compared with experimental data [25]. Johnson and his co-workers [26] have developed a method for applying the PI technique directly to GCMC simulations. In this work, we have used both of the above techniques to perform the simulations.

We report the effects of the simulation method, potential model, slit pore size, temperature and pressure on the binary quantum separation and selectivity of the hydrogen isotopes. We note that such H_2/D_2 mixture equilibrium simulations for slit pores have never before been reported, and are important even to the case of kinetic molecular sieving by carbons, as the pore body, modelled here as slit-shaped, influences the capacity, and therefore the flux of the different species.

2. Simulation methods

We used two different potentials for the fluid–fluid interactions, namely, the Lennard-Jones (LJ)

$$U(r) = 4\varepsilon\left(\frac{\sigma^{12}}{r^{12}} - \frac{\sigma^{6}}{r^{6}}\right), \tag{1}$$

with $\sigma = 0.296$ nm and $\varepsilon = 34.2$ K following Buch et al. [27], and the Silvera and Goldman (SG) potential [28]. The SG potential has the form

$$\phi(r) = \exp\left[\alpha - \beta r - \gamma r^2\right] - \left[\frac{C_6}{r^6} + \frac{C_8}{r^8} + \frac{C_{10}}{r^{10}}\right] f_c(r) + \frac{C_9}{r^9} f_c(r), \tag{2}$$

where $f_c(r)$ is the damping function

$$f_c(r) = \begin{cases} \exp\left[-\left(\frac{r_c}{r} - 1\right)^2\right] & r < r_c \\ 1 & r \geq r_c. \end{cases} \tag{3}$$

The parameters used here in the SG potential are the same as those originally reported [28].

The 10-4-3 potential [29] is used for the interaction of the adsorbate molecules with carbon slit pores, as given below,

$$v_{sf}(z) = 2\pi\rho_s\varepsilon_{sf}\sigma_{sf}\Delta\left[\frac{2\sigma_{sf}^{10}}{5z^{10}} - \frac{\sigma_{sf}^{4}}{z^4} - \frac{\sigma_{sf}^{4}}{3\Delta(z + 0.61\Delta)^3}\right], \tag{4}$$

where $\rho_{sf} = 114\,\text{nm}^{-3}$ is the number density of carbon atoms in graphite, $\Delta = 0.335$ nm is the distance between graphite layers, $\sigma_{sf} = 0.34$ nm and $\varepsilon_{sf} = 28$ K are the size parameter and energy well depth of the carbon–carbon LJ pair potential, and z is the distance between an adsorbate molecule and the surface of the wall. For a pore of width h, as depicted in Figure 1, the total solid–fluid interaction energy considering both pore walls is given by

$$V_{sf} = v_{sf}(z) + v_{sf}(h - z). \tag{5}$$

Here h is defined as the centre-to-centre distance between carbon atoms on the opposing surfaces, measured along the normal. The Buch parameters are used for hydrogen molecules to calculate the interactions with the pore walls. Lorentz–Berthelot mixing rules are applied for the calculation of the adsorbate–adsorbent cross-interaction LJ pair potential parameters.

The quantum effects are simulated by two different approaches. The first approach is the Feynman and Hibbs [19,20] effective potential approximation, which adds additional perturbation terms of quantum corrections to the original potential model. The FH approximation has been utilised for estimating the quantum effects in nanoporous materials in previous studies [3,4,12].

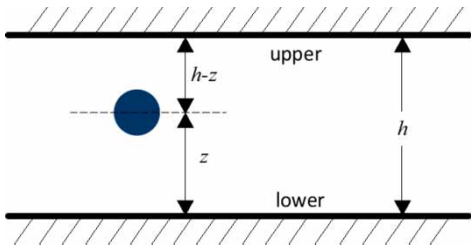

Figure 1. Schematic of a hydrogen molecule adsorbed in a carbon slit pore. h is the height of the slit pore and z is the distance between the molecule and the lower carbon wall.

The formalism takes the following form

$$U_{\mathrm{FH}}(r) = \left(\frac{6\mu}{\pi\beta\hbar^2}\right)^{3/2} \int \mathrm{d}R U(|\mathbf{r}+\mathbf{R}|) \times \exp\left(-\frac{6\mu}{\beta\hbar^2}R^2\right). \quad (6)$$

To counter the computational difficulties of Equation (6), it is common to expand $U(|\mathbf{r}+\mathbf{R}|)$ around $\mathbf{r}$ and suitably truncate the expansion. We used the fourth order approximation of Kumar and Bhatia [3,4] for better accuracy in the confined space, compared to the earlier quadratic approximation commonly used for the bulk fluid [30,31]. The fourth order approximation is given as

$$U_{\mathrm{FH}}(r) = U(r) + \frac{\beta\hbar^2}{24\mu}\left[U''(r) + \frac{2U'(r)}{r}\right] + \frac{\beta^2\hbar^4}{1152\mu^2}\left[\frac{15U'(r)}{r^3} + \frac{4U'''}{r} + U''''(r)\right], \quad (7)$$

where $\beta = 1/kT$, $\hbar$ is the Dirac constant and μ is the reduced mass, following

$$\mu = \frac{m_1 \times m_2}{m_1 + m_2}. \quad (8)$$

For carbon slit pores, the mass (m_2) can be considered as large compared to the mass of hydrogen molecules (m_1), which leads to $\mu \approx m_1$. $U_{\mathrm{FH}}(r)$ is either the LJ potential or the 10-4-3 potential for fluid–fluid and solid–fluid interactions, respectively.

The second approach used is the Feynman's PI formalism [23,24]. This method treats a single molecule as a ring of multiple beads. The adjacent beads in a ring are connected via harmonic springs. The spring constant k is calculated using

$$k = \frac{Pm}{(\beta\hbar)^2}, \quad (9)$$

where P is the number of beads per molecule, m is mass, $\beta = 1/k_{\mathrm{B}}T$ (k_{B} is the Boltzman constant) and $\hbar$ is the Dirac constant. The total energy is given by

$$U_{PI}(r) = \frac{1}{2}k\sum_{i=1}^{N}\sum_{\alpha=1}^{P}\left(r_i^{(\alpha)} - r_i^{(\alpha+1)}\right)^2 + \frac{1}{P}\sum_{i<j}\sum_{\alpha=1}^{P}U\left(r_{ij}^{(\alpha\beta)}\right), \quad (10)$$

where N is the number of molecules, P is the number of beads for each molecule, $r_i^{(\alpha)}$ is the position vector of the αth bead in the ith molecule ($\alpha + 1 = 1$ when $\alpha = P$), and $\mathbf{r}_{ij}^{(\alpha)}$ is the distance between the αth bead of two interacting ring polymers i and j, and $U(r_{ij}^{(\alpha)})$ the corresponding interaction energy. Inter-bead interactions are calculated using either the LJ or SG potential. The LJ potential with the Buch parameters is used for carbon atom–bead interactions.

We performed simulations in the grand canonical ensemble. The simulations consisted of two types of moves, translational movement and molecule insertion/deletion. For simulations using the PI method, we used a hybrid Monte Carlo method [32] to treat the translational movements of the molecules, as the ring polymer structure of the molecules leads to difficulties in movement using the simple random walk method. For each hybrid Monte Carlo move, the velocities are firstly drawn from a Gaussian random distribution based on the system temperature. Secondly, the forces for both intra- and inter-molecular interactions are calculated. Finally, the positions and velocities of all the molecules in the system are evolved via a velocity-Verlet [33] molecular dynamics algorithm. We have also used multiple-time-step simulation techniques to ease the intra-molecular movement. The intra-molecular interactions (composed of stiff harmonic springs) are calculated in the inner loop with a short time step. The inter-molecular interactions are calculated in the outer loop with a long time step. In order to achieve ergodicity for molecule insertions, a regular molecular dynamics simulation for ideal hydrogen at system temperatures runs in parallel with the adsorption simulations. The configuration of the inserted molecule is randomly chosen from the ideal gas system. Further, since the state variable specified for the simulations is the fugacity this was converted to pressure using the virial formula, for the purpose of depicting the isotherms.

In general, 200,000 steps are used for equilibrium and 500,000 steps are used for production runs at 77 K. At 40 K, we used 5×10^6 steps for equilibration and 10×10^6 for the data gathering. Each step is either a translational movement, molecule creation, or a deletion, with probabilities of 0.02, 0.49 and 0.49, respectively. In the PI simulations, the translational movement typically consisted of five molecular dynamics moves with 20 inner time steps for each long time step. The number of beads are set to be 30 for every absorbate molecule, which is sufficiently large for obtaining accurate results at the temperatures used [1,8,9,26].

The selectivity is calculated using the commonly used definition

$$S_{21} = \frac{x_2/x_1}{y_1/y_2}, \quad (11)$$

where S_{21} is the selectivity of component 2 over component 1, x_i is the mole fraction of the ith component in the adsorption phase and y_i is the mole fraction of the ith component in the bulk phase. Here component 2 is taken as D_2 and component 1 as H_2. We estimate the uncertainty of the selectivity calculations to be around 10%.

3. Results and discussion

3.1 Bulk phase simulations

We first performed simulations for bulk H_2, in order to verify the performance of different potential models used in this work. The simulations have been carried out at 77 K as well as at a lower temperature of 40 K. The result at 77 K is shown in Figure 2, comparing the model predictions with exact literature results using Younglove's 32-constant modified Benedict–Webb–Rubin equation of state for hydrogen [34].

The three combinations of simulation methods and potential models, namely FH with Buch parameters, PI with Buch parameters and PI with SG potential, all give results that match the experimental data very well at 77 K. Hence, all three combinations were further compared through adsorption simulations at this temperature. Since the temperature of 77 K is rather high for quantum effects to be very significant, we also performed the same series of simulations at a lower temperature of 40 K. The results are depicted in Figure 3, and reveal that only the PI simulations with SG potentials give accurate results at 40 K. The FH potential based simulations underestimate the H_2 densities, because the parameters for this option were not optimised here as done earlier by Kumar et al. [4]. Both PI based simulations are able to reproduce the bulk H_2 density reasonably. However, the PI simulations with SG potential have better accuracy over the entire pressure range. Therefore, only the PI simulations with SG potential were used for the subsequent binary adsorption investigations in carbon slit pores at 40 K.

3.2 Adsorption in carbon slit pores

We have performed adsorption simulations in carbon silt pores of various widths at both 77 and 40 K. The selectivity and adsorbed density were calculated via the simulations. The density is calculated as follows:

$$\rho_{\text{adsorbate}} = \frac{m_{\text{adsorbate}}}{l \times w \times h}, \tag{12}$$

where l, w and h are the length, width and height of the carbon slit pore used in the simulation, respectively. We have investigated the influence of slit pore size, temperature, pressure as well as simulation method and potential model on the separation process. The results are discussed in detail in the rest of this article. We used a 1:1 bulk composition ratio between H_2 and D_2 in the simulations. The optimal simulation method, potential model, slit pore size, temperature and pressure for efficient separations have been obtained through the simulations. A practical separation, based on 99.95% H_2 in the bulk phase, is also simulated using the optimal conditions.

3.2.1 Simulation method and potential model discrimination

We performed three sets of simulations at 77 K and 10 bar using the three combinations of simulation methods and potential models. The results are shown in Figure 4. Although the bulk simulation results showed that all of the three sets of simulations give very similar results, the adsorption simulations in slit pores using the FH approximation with the Buch parameters greatly overestimates selectivities for narrow slit pores. The PI simulations with the Buch parameters and SG potential models give very similar results. At the narrow pore sizes of $h = 0.54$ and 0.55 nm, the two simulation methods, FH and PI, yield results differing by factors of seven and four, respectively. In contrast, results of all three simulation sets match very well for large slit pore sizes, and at $h = 2.0$ nm, they are almost identical. The reason why FH fails

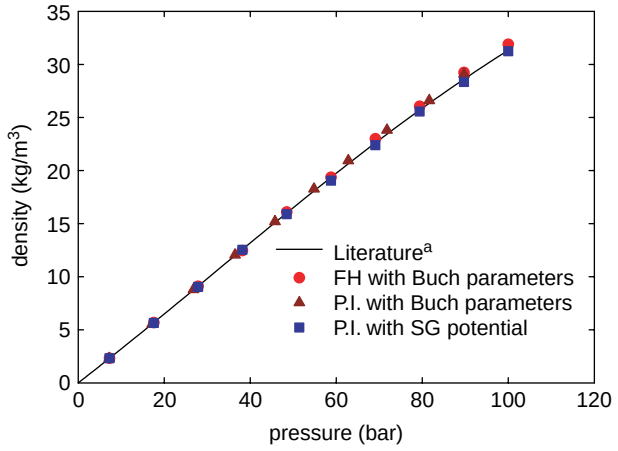

Figure 2. GCMC simulation results for bulk H_2 at 77 K. [a]Literature values are based on the Younglove equation of state for hydrogen [33].

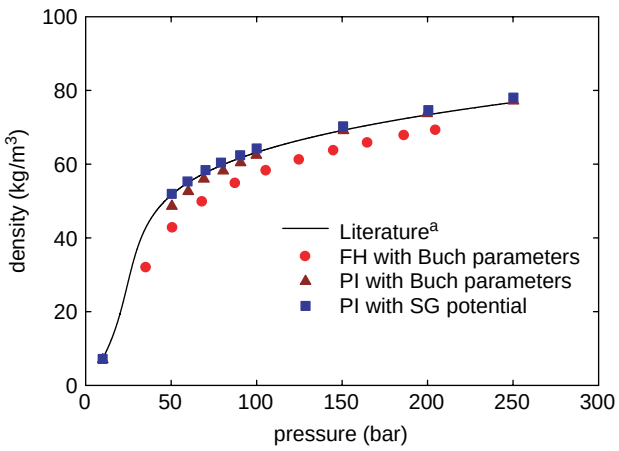

Figure 3. GCMC simulations results for bulk H_2 at 40 K. [a]Literature values are based on the Younglove equation of state for hydrogen [33].

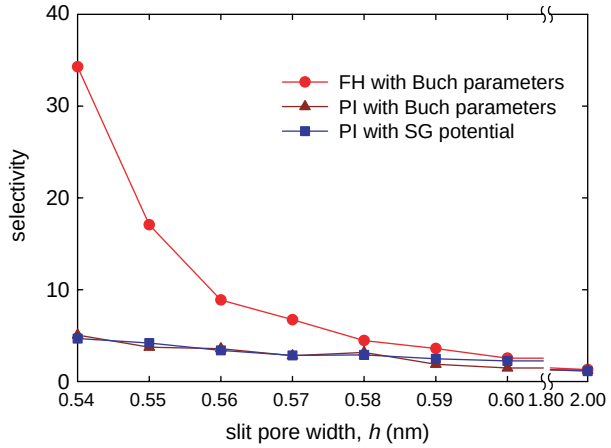

Figure 4. Comparison of different simulation methods and potential models for hydrogen separation in carbon slit pores at 77 K.

to correctly calculate the selectivities for very narrow slit pores is related to the highly confined environment, as a result of which the quantum time scale is no longer negligible in comparison to the time scale of the particle motion between collisions. The FH potential approximation integral formulation neglects motion on the quantum time scale [20] and is therefore not appropriate for such low temperatures or very strongly confined systems. As the slit pore size increases, the FH results become more reliable and match those from PI simulations. Since we are only interested in the narrow slit pores with high selectivities, the FH approximation is not considered suitable for the simulations. Although simulations using PI with Buch parameters give similar results as those using PI with SG potential at 77 K, we chose only PI with SG potential to perform our subsequent simulations in this work. This is because only simulations using PI with SG potential accurately reproduced the density for bulk hydrogen at 40 K.

3.2.2 *Effect of slit pore size*

The size of slit pores is critical to the separation of H_2 and D_2, and has an effect on both the adsorption density and selectivity. We have used slit pores with sizes ranging from 0.54 to 2.0 nm to show the effects, and the results are depicted in Figure 5. For both temperatures used, starting from $h = 0.54$ nm, the selectivity drops very rapidly with increasing slit pore width, h. For slit pore width greater than 0.6 nm, the selectivity curves show a plateau with values close to 1, indicating that separation becomes inefficient for such large slit pores. At the lower temperature of 40 K, the selectivity for D_2 is typically an order of magnitude larger than that at 77 K. This is due to the significantly larger de Broglie wave length of the lighter H_2 ($\sim$0.194 nm) compared to that of D_2

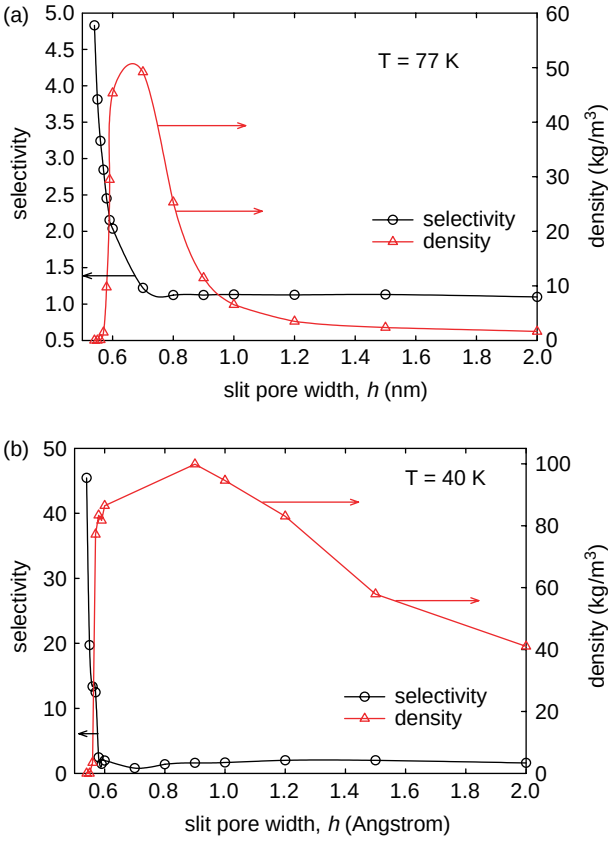

Figure 5. Effects of slit pore size on selectivity and density at (a) 77 K and (b) 40 K. In both cases, bulk pressure, P, is 0.1 bar. Arrows are guides to the eye to the corresponding ordinate for the curves.

($\sim$0.137 nm) at 40 K, while this difference is less significant at 77 K ($H_2 \sim 0.140$ nm and $D_2 \sim 0.099$ nm). As a result of the larger quantum uncertainty, the H_2 molecule appears swollen relative to D_2, and this difference is enhanced at the lower temperature of 40 K leading to the larger selectivity at this temperature.

Peaks can be observed around $h = 0.8$ nm for the density curves at both 77 and 40 K; however, at this size the selectivity is close to unity and the separation is inefficient. For very narrow slit pores, e.g. $h = 0.54$ nm, the densities are virtually zero for both temperatures, indicative of repulsive solid–fluid interactions. With increase in the slit pore width, adsorbed molecules form a single layer in the pores and the density increases due to the more favourable adsorbate–adsorbent interactions; however, when the slit pore width is very large, the pore potential becomes weaker and the density is reduced. In this condition, the adsorbate molecules form monolayers on the pore walls at the lower pressure of 0.1 bar as illustrated in Figure 6(b), with a very low density in the inner core. When the slit pore is narrow, adsorbate molecules stay at the centre of the slit pore, while interacting with both walls of the carbon pore, as seen

in Figure 6(a). Figure 7 depicts snapshots of the mixture adsorption in carbon slit pores with $h = 0.6$ and 2.0 nm. The layering on the walls evident in this figure is consistent with the findings of Kowalczyk et al. [17] and Wang and Johnson [10]. We note here that the pressure (0.1 bar) used in the simulations is rather low, and we therefore observe only the formation of monolayers in the slit pores.

Figure 6 also shows the mole fraction ratio of D_2/H_2 relative to the position. When $h = 0.6$ nm, the ratio has an obvious concave shape with a minimum located at the center for the slit pore, as seen in Figure 6(a). The minimum has a value of about 2.0 which is close to the overall selectivity of D_2 over H_2 at this condition. The mole fraction of D_2 becomes higher when moving towards the carbon pore walls. This is because the more swollen H_2 molecule has larger de Broglie wavelength and tends to stay further away from the carbon pore walls than D_2 molecules. This behaviour is still observable in Figure 6(b) for the large carbon slit pore with $h = 2.0$ nm. Two peaks are located at both ends of the ratio curve, despite large scatter in the interior. The average ratio is about unity at the centre of the pore, as indicated by the reference line, implying poor selectivity at this large pore size.

As seen in Figure 5, the selectivity curves become relatively flat at a pore width of around 0.6 nm. We therefore chose narrow slit pores with width smaller than 0.6 nm in further simulations. The results are shown in Figures 8 and 9. Figure 8 shows that the selectivity decreases with increase in h. This is the case for both of the temperatures, and various pressures up to 10 bar. At 40 K the selectivities are greater than those at 77 K by almost an order of magnitude, due to the larger quantum effects on the H_2, as discussed above. The pressure does not affect the selectivity significantly and the trend is less significant in Figure 8, compared to that of slit pore size and temperature. The effects of pressure and temperature will be discussed in detail in subsequent sections.

In contrast to the selectivity, the total adsorbed density increases with slit pore size, as shown in Figure 9. The plateau regions in Figure 9(b) indicate that adsorption has reached saturation, and this occurs at about 0.57 nm at the lower temperature of 40 K. A high selectivity as well as high density are necessary to make the separation process more efficient. We conclude that the optimal slit pore size is 0.56 nm for both 77 and 40 K based on our calculations, with a pressure of about 1.0 bar at 40 K, at which point the total adsorbed density is high and selectivity for D_2 is about 16.58 at 40 K.

3.2.3 *Effect of pressure*

As discussed in the previous section, higher pressure increases the adsorbate density. However, the selectivity does not show an obvious trend with variation of pressure. Therefore, we investigated the variation of the selectivity

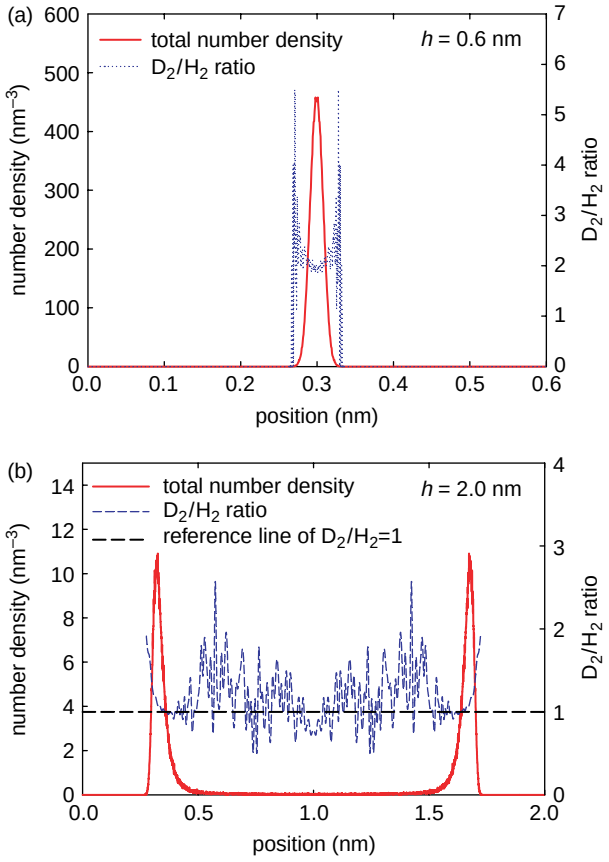

Figure 6. Total density profiles and D_2/H_2 mole ratio for H_2/D_2 mixture adsorption in carbon slit pores of width (a) 0.6 nm and (b) 2.0 nm. Pressure is 0.1 bar and temperature is 77 K, with a 1:1 bulk H_2/D_2 mixture. The position is the normal distance measured from the lower wall.

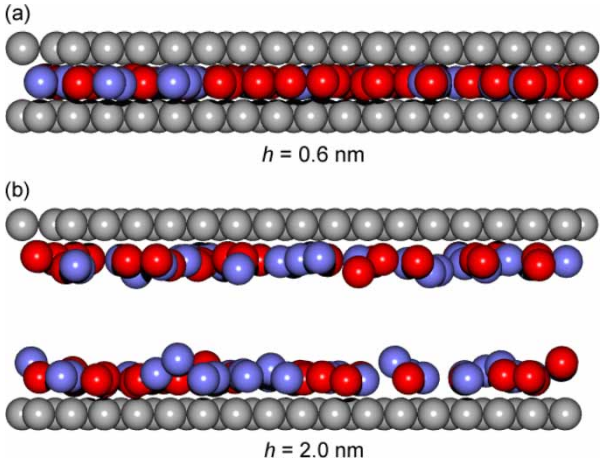

Figure 7. Snapshots of H_2/D_2 mixture adsorption in carbon slit pores of width (a) $h = 0.6$ nm and (b) $h = 2.0$ nm. The gray spheres are carbon atoms. The blue spheres are hydrogen molecules. The red spheres are deuterium molecules. Bulk conditions are the same as for Figure 6.

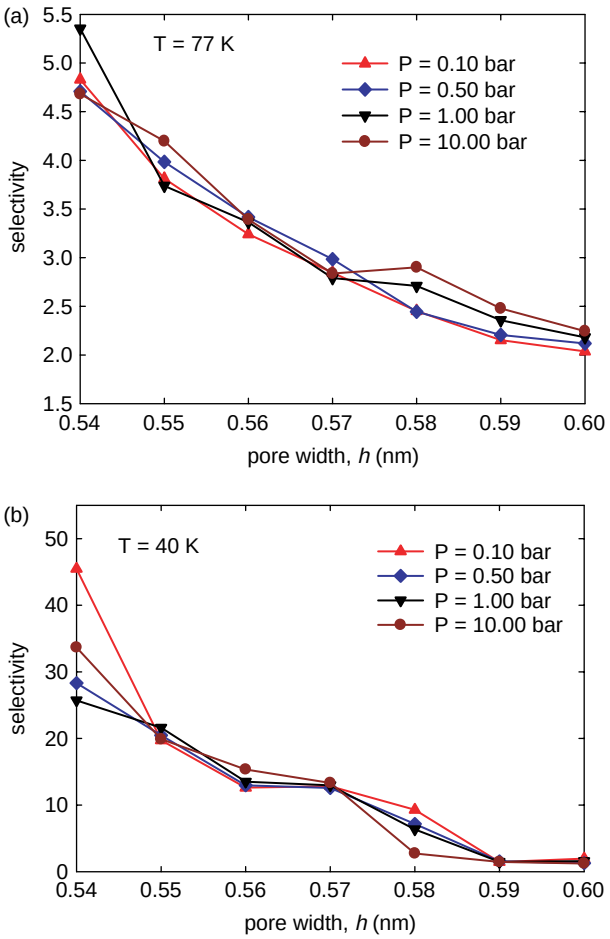

Figure 8. Variation of selectivity with slit pore width at (a) 77 K and (b) 40 K.

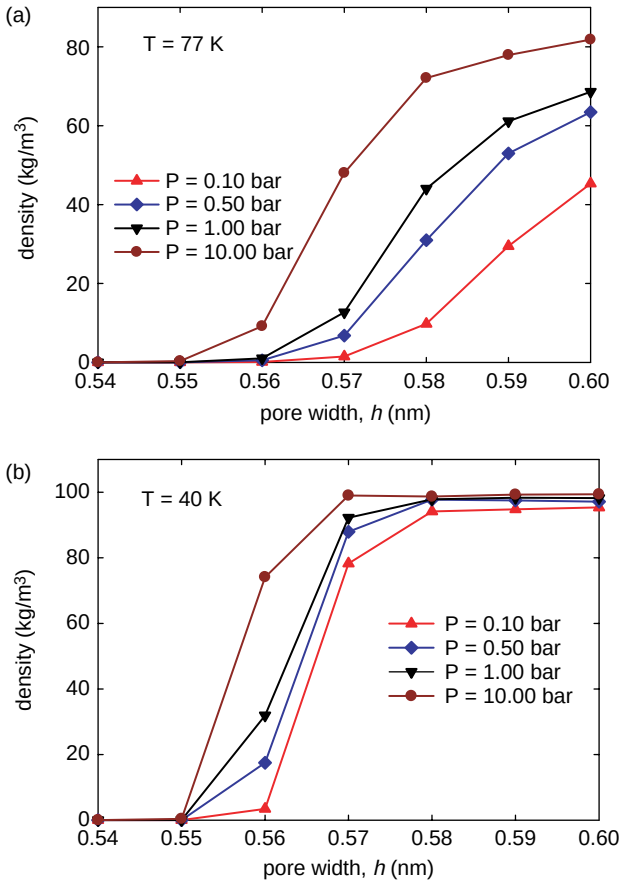

Figure 9. Variation in total adsorbed density with slit pore width at (a) 77 K and (b) 40 K.

and density with pressure in more detail. The results are shown in Figures 10 and 11.

As seen in Figure 10, the selectivity is not sensitive to the pressure at 77 K, despite some scatter. We note that the range of the selectivity axis is small in Figure 10(a) (covering a factor of only 3.5). Therefore the scatter is not considered and, given the accuracy of the simulations, it does not reflect any physical features. Therefore, a general trend is not discernible based on the results. This is consistent with the findings of Garberoglio [18], where he stated the selectivity remains almost constant over the pressure range at 77 K. At 40 K, the results for pore of size of 0.58 nm show an inverse relation between pressure and selectivity. However, the results for pores of sizes of 0.56 and 0.57 nm appear to show a roughly positive relation between pressure and selectivity, as linear trend lines of positive slope can be drawn for the curves. Due to the large scatter we noted in previous section (10%), there are some points that do not agree with the positive relation. The positive relation for the pore size of 0.57 nm is in agreement with Garberoglio's study [18]. For larger slit pore width of 0.6 nm in Figure 10(b), the adsorption reaches saturation and the selectivities are close to unity and insensitive to the pressure. These findings differ from the result of Challa et al. [1], where a positive relation is shown between selectivity and pressure at all conditions. This is possibly because different pressure ranges are used in their calculations (mostly under 10^{-3} torr). In addition, the systems (nanotube interior sites and interstices) used in their simulations are pseudo-one-dimensional, while the carbon slit pore is pseudo-two-dimensional.

At 40 K, the density consistently increases with increase in pressure. Although only pure hydrogen was used in studies of Kowalczyk et al. [17], our density results at 77 K match their results well in both the trend and the order of different size of pores in respect of the density, indicating these two features are not sensitive to the isotope difference. We note that we have used a logarithmic scale for the pressure, therefore the curves have opposite concavity to what has been shown in Kowalczyk et al. [17]. Since we have set the optimal slit pore size to be 0.56 nm, we chose the optimal pressure for

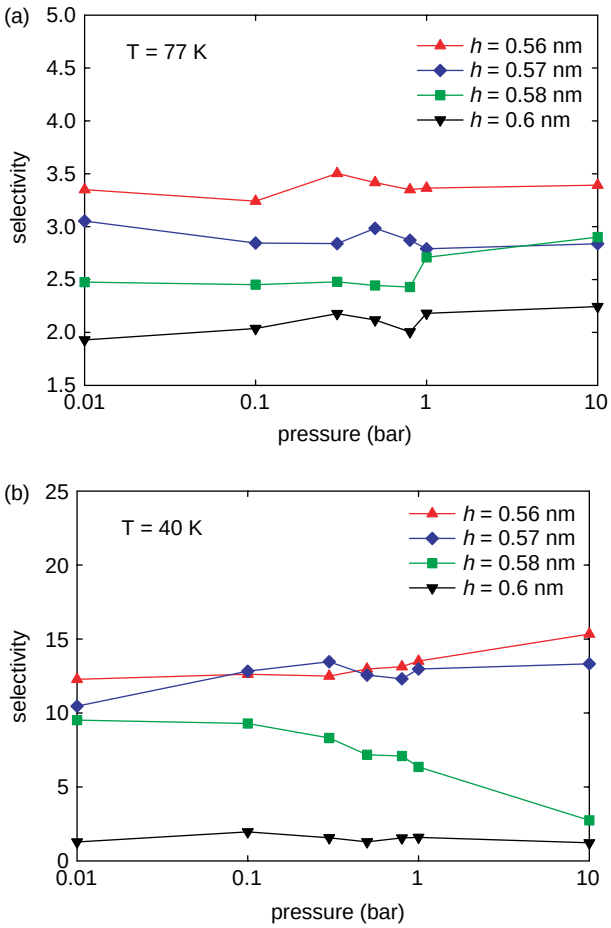

Figure 10. Variation of selectivity with pressure at (a) 77 K and (b) 40 K, for various pore widths.

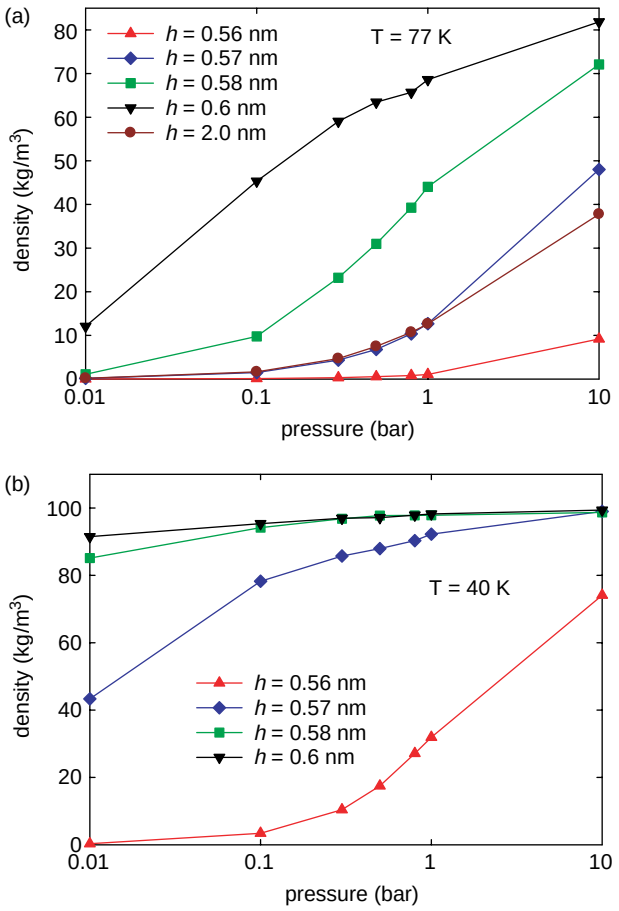

Figure 11. Variation in total adsorbed density with pressure at (a) 77 K and (b) 40 K, for various pore widths.

this slit pore size with the standard of high selectivity and high density. The optimal pressures would appear to be 10 bar for both 77 and 40 K. However, considering the large scatter in the selectivity data, the difference in the selectivities between 1.0 and 10 bar for 0.56 nm slit pore at 40 K can be possibly due to the calculation uncertainty. Therefore, the lower pressure of 1.0 bar is also a good choice for the optimal pressure due to the smaller compression cost.

3.2.4 *Effect of temperature*

Quantum effects are more prominent at lower temperatures. Therefore it is expected that the separation process is more efficient at 40 K than that at 77 K. The detailed results for the optimal conditions are listed in Table 1 for both 40 and 77 K.

The selectivity and density are both significantly higher at 40 K. This is consistent with what is expected. The radius of gyration (R_g) has also been calculated for the ring polymer used in the simulations as an indicator of quantum effects. The calculation of mean radius of gyration is based on the definition.

$$\langle R_g(P)\rangle = \frac{1}{P}\left\langle \sum_{i=1}^{P} |\boldsymbol{r}_i - \boldsymbol{r}_{cm}| \right\rangle, \tag{13}$$

where $\boldsymbol{r}_{cm} = 1/P\sum_{i=1}^{P}\boldsymbol{r}_i$ is the centre of mass of the ring polymer, r_i is the position vector of ith bead in the ring, and P is the number of beads in each ring. Larger R_g implies a stronger quantum effect. The value of R_g for D_2 is always smaller than that of H_2 at the same temperature. This is the reason for the observation of the separation of the two molecules in narrow slit pores. This also consolidates our explanations of the larger D_2/H_2 mole fraction ratio close to the pore walls in Figure 6. While the temperature increases, the R_g values of both H_2 and D_2 drop and lead to weaker quantum effects. This in turn results in lower selectivity. Therefore, 40 K is a better choice of temperature compared to 77 K.

3.2.5 *Simulation of practical separation*

Having determined the appropriate simulation method (PI) and potential model (SG), as well as optimal slit pore size (0.56 nm), pressure (1.0 bar) and temperature (40 K),

Table 1. Comparison of selectivity, density and radius of gyration (R_g) for 40 and 77 K at optimal conditions.

	Simulation method and potential model	Slit pore height (nm)	Pressure (bar)	Selectivity	Density (kg/m^3)	R_g of H_2 (nm)	R_g of D_2 (nm)
40 K	PI with SG	0.56	1.0	16.58	33.22	0.0319	0.0238
77 K	PI with SG	0.56	10.0	3.39	9.18	0.0251	0.0181

Table 2. Separation of H_2/D_2 mixture in carbon slit pore ($h = 0.56$ nm) with 0.05% D_2 as initial bulk concentration, at $T = 40$ K and $P = 1.0$ bar.

	Selectivity	Mole fraction of D_2 (%)	Density (kg/m^3)
First separation	12.52	0.62	2.62
Second separation	11.64	6.79	3.20
Third separation	13.95	50.3	6.74

we performed simulations using a bulk gas composition of 99.95% H_2 and 0.05% D_2. This proportion of deuterium corresponds to that for hydrogen gas in nature. The simulations showed strong separation capability of narrow slit pores for H_2/D_2. The results are shown in Table 2.

The second separation uses the mole fraction calculated from the first separation as the bulk composition. Similarly, the third separation uses the mole fraction from the second separation. We are able to achieve 50.3% D_2 concentration after only three separation steps. Thus, the D_2 concentration is increased over 1000 times. This result indicates efficient separation of H_2/D_2 using narrow carbon slit pores as the adsorption medium at low temperature. The quantum effect plays a critical role in the separation process. Bhatia and co-workers [3–5] have reported kinetic molecular sieving of hydrogen isotopes in zeolite rho due to a reverse relation between the diffusivity and the quantum effect, which remarkably leads to the heavier deuterium diffusing faster than the lighter hydrogen at sufficiently low temperature. This result can be combined with our findings. The large equilibrium adsorption selectivity of D_2 shown in this work leads to high adsorbed amount of D_2 in narrow carbon slit pores, which in turn leads to large flux of D_2. With the aid of faster diffusion, more efficient quantum molecular sieving (i.e. flux selectivity) can be achieved.

4. Conclusions

Both selectivity and adsorbate density must be considered while choosing the conditions for an efficient separation process. Low selectivity causes poor separation between H_2 and D_2. Low adsorbate density implies poor utilisation of the adsorbent, which could make the process uneconomical. In general, narrow slit pore sizes and low temperature are favourable for efficient separation. The pressure does not show a strong effect on the selectivity. However, higher pressure helps to increase the adsorbate density. Therefore, in the pressure range that we have tested, moderately high pressures are chosen as optimal (1.0 bar for 40 K and 10 bar for 77 K). The radius of gyration calculations show consistent trend with changes of the selectivity.

The series of separation simulations starting with 99.95% H_2 concentration show highly efficient separation of H_2/D_2 in a carbon slit pore having width equal to 0.56 nm at 40 K and 1.0 bar. The efficiency of the separation process can possibly be further improved by the faster diffusion of D_2 compared to H_2 at low temperature. We note that the simulations have been performed for a single carbon slit pore. The real material will comprise a distribution of pore widths, with additional complexities in structure and connectivity. Therefore, the real separation efficiency may somewhat differ from the calculations. However, the theory and general trends that we have observed from the simulations will still apply to the real separation processes.

Acknowledgements

The authors thank Professor J. Karl Johnson, Dr Giovanni Garberoglio and Dr Jinchen Liu for helpful discussions. This research has been supported by a grant from the Australian Research Council under the Discovery Scheme.

References

[1] S.R. Challa, D.S. Sholl, and J.K. Johnson, *Adsorption and separation of hydrogen isotopes in carbon nanotubes: multi-component grand canonical Monte Carlo simulations*, J. Chem. Phys. 116(2) (2002), pp. 814–824.
[2] S.R. Challa, D.S. Sholl, and J.K. Johnson, *Light isotope separation in carbon nanotubes through quantum molecular sieving*, Phys. Rev. B 63 (2001), pp. 245–419.
[3] A.V.A. Kumar and S.K. Bhatia, *Quantum effect induced reverse kinetic molecular sieving in microporous materials*, Phys. Rev. Lett. 95 (2005), p. 245901, Erratum: 245996 (242006), p. 119901.
[4] A.V.A. Kumar, H. Jobic, and S.K. Bhatia, *Quantum effects on adsorption and diffusion of hydrogen and deuterium in microporous materials*, J. Phys. Chem. B 110 (2006), pp. 16666–16671.

[5] A.V.A. Kumar and S.K. Bhatia, *Is kinetic molecular sieving of hydrogen isotopes feasible?*, J. Phys. Chem. C 112 (2008), pp. 11421–11426.
[6] G. Garberoglio, M.M. Deklavon, and J.K. Johnson, *Quantum sieving in single-walled carbon nanotubes: effect of interaction potential and rotational–translational coupling*, J. Phys. Chem. B 110 (2006), pp. 1733–1741.
[7] Q. Wang, S.R. Challa, D.S. Sholl, and J.K. Johnson, *Quantum sieving in carbon nanotubes and zeolites*, Phys. Rev. Lett. 82(5) (1999), pp. 956–959.
[8] G. Garberoglio, A.I. Skoulidas, and J.K. Johnson, *Adsorption of gases in metal organic materials: comparison of simulations and experiments*, J. Phys. Chem. B 109 (2005), pp. 13094–13103.
[9] Q. Wang and J.K. Johnson, *Hydrogen adsorption on graphite and in carbon slit pores from path integral simulations*, Mol. Phys. 95(2) (1998), pp. 299–309.
[10] Q. Wang and J.K. Johnson, *Molecular simulation of hydrogen adsorption in single-walled carbon nanotubes and idealized carbon slit pores*, J. Chem. Phys. 110(1) (1999), pp. 577–586.
[11] J. Liu, J.T. Culp, S. Natesakhawat, B.C. Bockrath, B. Zande, S.G. Sankar, G. Garberoglio, and J.K. Johnson, *Experimental and theoretical studies of gas adsorption in $Cu_3(BTC)_2$: an effective activation procedure*, J. Phys. Chem. C 111 (2007), pp. 9305–9313.
[12] H. Tanaka, H. Kanoh, M. El-Merraoui, W.A. Steele, M. Yudasaka, S. Iijima, and K. Kaneko, *Quantum effects on hydrogen adsorption in internal nanospaces of single-wall carbon nanohorns*, J. Phys. Chem. B 108 (2004), pp. 17457–17465.
[13] Y. Hattori, H. Tanaka, F. Okino, H. Touhara, Y. Nakahigashi, S. Utsumi, H. Kanoh, and K. Kaneko, *Quantum sieving effect of modified activated carbon fibers on H_2 and D_2 adsorption at 20 K*, J. Phys. Chem. B 110 (2006), pp. 9764–9767.
[14] H. Tanaka, H. Kanoh, M. Yudasaka, S. Iijima, and K. Kaneko, *Quantum effects on hydrogen isotope adsorption on single-wall carbon nanohorns*, J. Am. Chem. Soc. 127(20) (2005), pp. 7511–7516.
[15] J.J.M. Bennakker, V.D. Borman, and S.Y. Krylov, *Molecular transport in subnanometer pores: zero-point energy, reduced dimensionality and quantum sieving*, Chem. Phys. Lett. 232(4) (1995), pp. 379–382.
[16] X. Zhao, S. Villar-Rodil, A.J. Fletcher, and K.M. Thomas, *Kinetic isotope effect for H_2 and D_2 quantum molecular sieving in adsorption/desorption on porous carbon materials*, J. Phys. Chem. B 110 (2006), pp. 9947–9955.
[17] P. Kowalczyk, P.A. Gauden, A.P. Terzyk, and S.K. Bhatia, *Thermodynamics of hydrogen adsorption in slit-like carbon nanopores at 77 K. Classical versus path-integral Monte Carlo simulations*, Langmuir 23 (2007), pp. 3666–3672.
[18] G. Garberoglio, *Boltzmann bias grand canonical Monte Carlo*, J. Chem. Phys. 128 (2008), p. 134109.
[19] R.P. Feynman, *Statistical Mechanics: a Set of Lectures*, WA Benjamin, Reading, MA, 1972.
[20] R.P. Feynman and A.R. Hibbs, *Quantum Mechanics and Path Integrals*, McGraw-Hill, New York, 1965.
[21] L.M. Sesé, *Study of the Feynman–Hibbs effective potential against the path-integral formalism for Monte Carlo simulations of quantum many-body Lennard-Jones systems*, Mol. Phys. 81(6) (1994), pp. 1297–1312.
[22] L.M. Sesé, *Feynman–Hibbs potentials and path integrals for quantum Lennard-Jones systems: theory and Monte Carlo simulations*, Mol. Phys. 85(5) (1995), pp. 931–947.
[23] R.P. Feynman, *Space-time approach to non-relativistic quantum mechanics*, Rev. Mod. Phys. 20 (1948), pp. 367–387.
[24] D. Landau and K. Binder, *A Guide to Monte Carlo Simulations in Statistical Physics*, Cambridge University Press, Camridge, UK, 2000.
[25] Q. Wang, J.K. Johnson, and J.Q. Broughton, *Thermodynamic properties and phase equilibrium of fluid hydrogen from path integral simulations*, Mol. Phys. 89(4) (1996), pp. 1105–1119.
[26] Q. Wang, J.K. Johnson, and J.Q. Broughton, *Path integral grand canonical Monte Carlo*, J. Chem. Phys. 107 (1997), pp. 5108–5117.
[27] U. Buch, F. Huisken, A. Kohlhase, and D. Otten, *Path integral simulations of mixed* para-D_2 *and* ortho-D_2 *clusters: the orientational effects*, J. Chem. Phys. 100 (1994), pp. 7610–7629.
[28] I.F. Silvera and V.V. Goldman, *The isotropic intermolecular potential for H_2 and D_2 in the solid and gas phases*, J. Chem. Phys. 69 (1978), pp. 4209–4213.
[29] W.A. Steele, *The physical interaction of gases with crystalline solids: I Gas–solid energies and properties of isolated adsorbed atoms*, Surface Sci. 36 (1973), pp. 317–352.
[30] B. Guillot and Y. Guissani, *Quantum effects in simulated water by the Feynman–Hibbs approach*, J. Chem. Phys. 108 (1998), pp. 10162–10174.
[31] N. Tchouar, F. Ould-Kaddour, and D. Levesque, *Computation of the properties of liquid neon, methane, and gas helium at low temperature by the Feynman–Hibbs approach*, J. Chem. Phys. 121 (2004), pp. 7326–7331.
[32] S. Duane, A.D. Kennedy, B.J. Pendleton, and D. Roweth, *Hybrid Monte Carlo*, Phys. Lett. B 195 (1987), pp. 216–222.
[33] M.P. Allen and D.J. Tildesley, *Computer Simulation of Liquids*, Oxford University Press, New York, 1987.
[34] B.A. Younglove, *Thermophysical properties of fluids. I. Argon, ethylene, parahydrogen, nitrogen, nitrogen trifluoride, and oxygen*, J. Phys. Chem. Ref. Data, Suppl. 11 (1982), pp. 1–349.